Full Paper Transactions, SMiRT 28
Toronto, Canada, August 10-15, 2025

Computational Models for Squat UHPC Shear Walls Reinforced with High-strength Steel

Yu-Hsin Cheng[1], Li-Yin Shen [1], Ping-Lun Hsieh[1], Chin-Cheng Lin[2] , and Chung-Chan Hung [3]

[1] Master student, Department of Civil Engineering, National Cheng Kung University, Taiwan (N66124246@gs.ncku.edu.tw, dear31303@gmail.com, rain811231@gmail.com)
[2] PhD student, Department of Civil Engineering, National Cheng Kung University, Taiwan (hugo790731@gmail.com)
[3]Distinguished Professor, Department of Civil Engineering, National Cheng Kung University, Taiwan (cchung@ncku.edu.tw)

ABSTRACT

The applications of ultra-high performance concrete (UHPC) and high-strength steel are effective strategies to enhance the shear resistance and resilience of structural walls. However, research on straightforward yet effective computational models for squat UHPC shear walls reinforced with high-strength steel remains limited. This study aimed to develop such models to predict the elastic, flexural, and shear behavior of squat UHPC shear walls. OpenSees was employed as the platform for developing the models.

In the developed model, nonlinear beam-column elements with fiber sections in OpenSees are employed to capture the flexural behavior of the walls. To simulate the shear behavior of the squat walls, spring elements are incorporated to represent both sliding-shear behavior and shear behavior, with the sliding-shear envelope calibrated using experimental data. Additionally, the shear force versus distortion behavior for the UHPC shear wall is calculated using the Modified Compression Field Theory (MCFT) proposed by Bentz et al. (2006).

The model's performance was validated against experimental results for UHPC shear walls conducted by Hung et al. (2017) and Hung and Hsieh (2020). The experimental variables of the shear walls included concrete type, reinforcement strength, and shear demand of the shear walls. The seismic behaviors of squat shear walls were evaluated through hysteretic behaviors under cyclic loadings. Findings demonstrated that the developed model reasonably captures the hysteretic behavior, lateral strength, stiffness, energy dissipation capacity, and shear sliding deformation of UHPC squat shear walls under various design configurations. Consequently, the proposed model offers an efficient and reliable method for predicting the hysteretic behavior of UHPC squat shear walls.

INTRODUCTION

Reinforced concrete shear walls are critical structural components to resist lateral forces effectively during seismic events, owing to their high stiffness and strength. However, squat shear walls are particularly vulnerable to shear failure during seismic loadings, highlighting the importance of material selection and cross-sectional design. High-strength materials, including ultra-high performance concrete and high-strength steel, are increasingly utilized in reinforced concrete structures with their superior mechanical performances to provide better shear resistance and resilience.

UHPC is an excellent alternative to conventional concrete with its exceptional mechanical properties. UHPC possesses compressive strength ranging from 100–150 MPa and tensile strength exceeding 7 MPa, primarily due to the bridging effects when fibers were pulled out of the matrix. Experimental studies by Hung and Hsieh (2020) have shown that steel fiber delayed the rapid strength degradation during post-peak loading, exhibiting UHPC’s superior stiffness, greater strength, enhanced confinement, crack-width control, and enhanced ductility, which confirms its advanced seismic performance. Additionally, these mechanical advantages provide the potential to reduce wall thickness, offering improved space utilization and significant social and economic benefits.

When high-performance concrete is used in structural wall constructions, applying high-strength steel reinforcement could reduce the number of steel bars and alleviate congestion during construction while delaying yielding of reinforcement. Furthermore, installing high-strength reinforcement could fully exploit the strength capacity despite the high nominal yield strength of the longitudinal and transverse reinforcement. The use of high-strength material, including UHPC hand high-strength steel, could enhance the structural members' lateral strength, stiffness, and ductility.

However, research on straightforward yet effective computational models for squat UHPC shear walls reinforced with high-strength steel remains limited. This study aimed to develop accurate and efficient models to predict the elastic, flexural, and shear behavior of squat UHPC shear walls with OpenSees. The model's performance was validated against experimental results for UHPC shear walls conducted by Hung et al. (2017) and Hung and Hsieh (2020), where the experimental variables include concrete type, reinforcement strength, and shear demand under a similar cross-sectional design configuration.

Under cyclic loading, experimental findings highlighted that UHPC shear walls outperformed conventional concrete walls in stiffness, strength, and ductility, indicating notable improvements in seismic performance. Similarly, simulation results reasonably capture the hysteretic behavior, lateral strength, and shear sliding deformation of UHPC shear walls with different designing parameters. These results confirm that the modeling methodology developed in this study is both efficient and effective.

MODEL ESTABLISHMENT

The model's performance was validated against experimental results for UHPC shear walls with a similar cross-section, as shown in Fig.1. Designing variables including 1) concrete type: high strength concrete (HSC) and UHPC with or without 1.5% volume fraction of steel fibers, 2) steel grade: SD420 and SD785. Specimens are labeled based on concrete type (HSC/UHPC), with or without steel fibers (SF), grade of reinforcement (NS and HS representing SD420 and SD785), and the shear demand ratio. For instance, UHPC-SF-HS-0.83$\sqrt{f_c'}$ refers to the wall specimen with UHPC containing steel fibers, reinforced with SD785 steel bars, and the shear demand ratio is 0.83$\sqrt{f_c'}$. Details of the specimen are listed in Table 1.

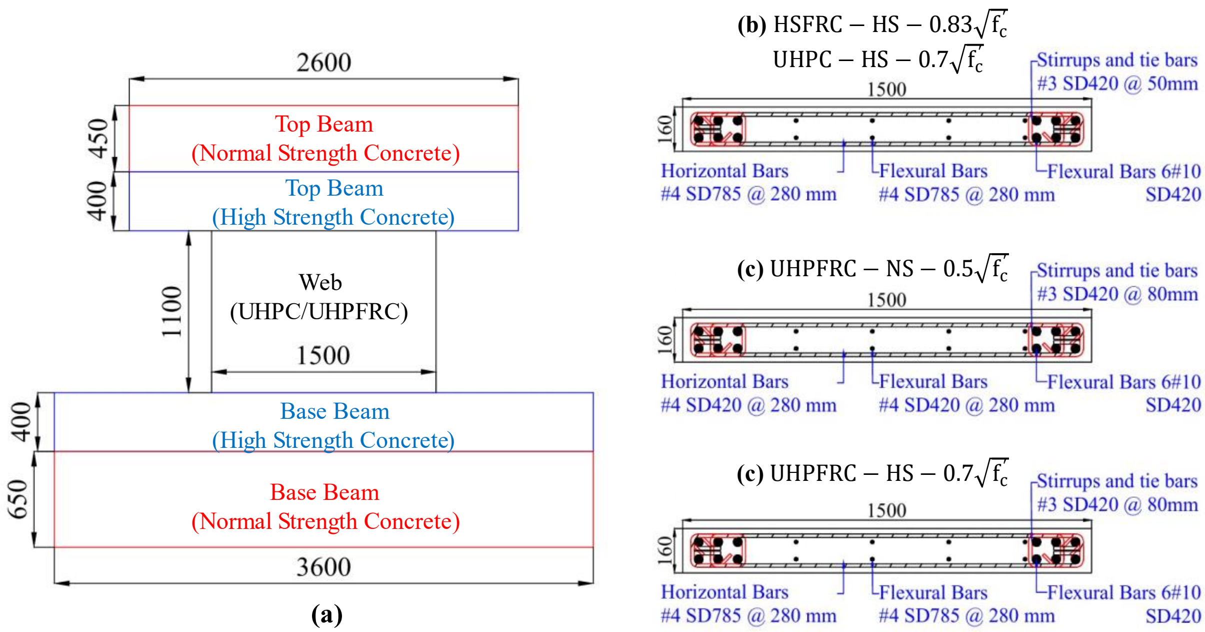

Fig. 1 (a) Setup of the squat shear wall (b)-(d) Setup of the wall cross-section

In the developed model, nonlinear beam-column elements with fiber sections in OpenSees are utilized to represent the flexural behavior of the walls, as illustrated in Fig.2. To capture the shear behavior of the squat shear walls, spring elements were integrated with zero-length element command to account for both sliding-shear behavior and shear behavior.

For matrix without steel fibers, the concrete fibers within the fiber section utilize the Concrete01 command, which follows the Kent–Scott–Park stress-strain model, according to Mazzoni et. al (2006). As for the matrix with 1.5% steel fibers, the ECC01 command that follows the constitutive law by Han et al. (2003) was incorporated to account for the tensile behavior and strain-hardening behavior of fiber-reinforced concrete. The stress-strain model in the Steel02 OpenSees command, proposed by Filippou et al. (1983), is used to simulate the steel reinforcement.

Table 1. Design parameters of the squat shear walls

	Horizontal Reinforcement	**Longitudinal Reinforcement**	**Flexural Bars At Boundary**	**Horizontal Bars At Boundary**
$\mathrm{HSC-HS}-0.83\sqrt{f_c'}$	8#4 (SD785)	8#4 (SD785)	6#10 (SD420)	#3 @50mm (SD420)
$\mathrm{UHPC-HS}-0.7\sqrt{f_c'}$	8#4 (SD785)	8#4 (SD785)	6#10 (SD420)	#3 @50mm (SD420)
$\mathrm{UHPC-SF-NS}-0.5\sqrt{f_c'}$	8#4 (SD420)	8#4 (SD420)	6#10 (SD420)	#3 @80mm (SD420)
$\mathrm{UHPC-SF-HS}-0.7\sqrt{f_c'}$	8#4 (SD785)	8#4 (SD785)	6#10 (SD420)	#3 @50mm (SD420)

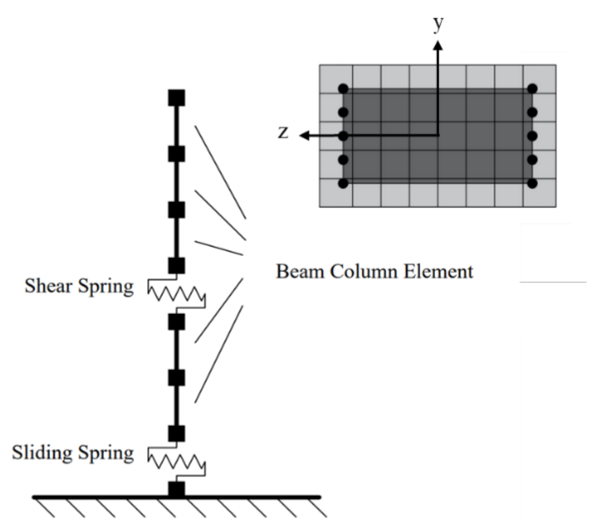

Fig. 2 OpenSees model setup

Shear Springs

The shear force versus shear strain behavior for the UHPC shear wall is evaluated using the simplified Modified Compression Field Theory (MCFT) proposed by Bentz et al. (2006). MCFT predicts the load-deformation response of reinforced concrete elements under in-plane shear and normal stress. This establishes an independent stress-strain relationship for cracked concrete through the integration of force equilibrium, compatibility, and constitutive law, accounting for the tensile behavior of cracked concrete. As the load-deformation relationship is derived, it is incorporated into the numerical model through the zero-length element command in OpenSees.

Sliding-Shear Springs

The sliding-shear behavior of the squat shear wall is incorporated into the computational model using the zero-length element, with the load-deformation relationship established based on TEASPA 3.1, ACI 318-14, and Eurocode 8. TEASPA 3.1 considers sliding-shear behavior a linear relationship for lateral forces below the maximum strength and is divided into two stages: before and after the maximum strength is reached. This could be further categorized into two responses, S1 and S2, as shown in Fig. 3. S1 represents the failure controlled by shear failure, and the fracture points were defined according to MCFT when the tensile strain of concrete reaches 0.015, or the principal strain reaches the compressive strain. S2 represents the failure when the squat shear walls are not subjected to shear failure, where the sliding deformation significantly increases due to the development of flexural cracks when the nominal flexural strength is reached. The fracture points were defined according to the fracture point by MCFT when the tensile strain of concrete reaches 0.015 or the principal strain reaches 0.003.

The springs are constituted of four points:

1. Flexural yielding point (δ_y, V_y):
   The yielding shear strength was derived from the moment-curvature analysis of OpenSees. The corresponding δ_y was calculated using TEASPA 3.1, as equation (1). Where h_w is the wall height between the base and the lateral load application point, d_b is the diameter of the tensile longitudinal bar at the wall boundary, f_{xy} is the yielding stress of the longitudinal bars, u is the average bonding stress suggested by Lehman and Moehle (2000), and a_c is the depth of the compression zone of the structural wall suggested by Paulay and Priestley (1992).
   $$\delta_y = \frac{d_b f_{xy}^2}{8uE_s(d-a_c)} h_w \tag{1}$$
2. Flexural strength point (δ_{mn}, V_{mn}):
   The nominal shear strength was derived from the nominal moment M_n value through moment-curvature analysis. The corresponding deformation is calculated based on the linear relationship, as equation (2).
   $$\delta_{mn} = \frac{V_{mn}}{V_y} * \delta_y \tag{2}$$
3. Sliding shear point (δ_f, V_f):
   The sliding shear point is derived according to ACI 318-14 when the shear-friction reinforcement is perpendicular to the shear plane. The μ is the coefficient of friction, A_{vf} is the area of reinforcement crossing the assumed shear plane, and the shear strength across the shear plane and the deformation is derived by equation (3)-(4).
   $$V_n = \mu A_{vf} f_y \tag{3}$$
   $$\delta_u = \frac{V_f}{V_y} * \delta_y \tag{4}$$
4. Fracture point: The fracture point is determined using MCFT criteria when the principal tensile strain or the principal compressive strain is reached.

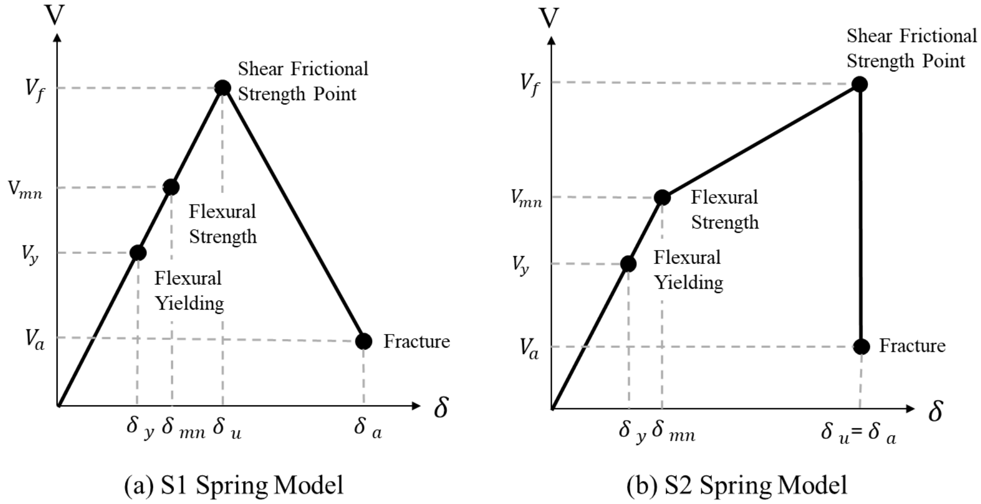

Fig. 3 Load-Deformation relationship of S1 and S2 sliding spring model

The shear resistance and resilience of the squat shear wall are inherently enhanced with UHPC, enabling the structural wall to sustain larger deformations during failure. Consequently, the flexural and shear strength will likely exceed the frictional shear strength, potentially leading to sliding failure mode.

In this study, the S3 spring is developed to represent the load-deformation response of the shear wall under sliding failure. Three linear stages characterize the response: 1) Before the frictional shear strength is reached; 2) After the frictional shear strength is reached and before the ultimate deformation is achieved; and 3) Post-ultimate deformation behavior. The response is further defined by four critical points:

1. Flexural yielding point (δ_y, V_y) derived from the moment-curvature analysis of OpenSees and the calculated δ_y value using TEASPA 3.1.
2. Flexural strength point (δ_{mn}, V_f) derived from the moment-curvature analysis of OpenSees and linear relationship with flexural yielding point.
3. Frictional shear strength (δ_u, V_f), where according to TEASPA 3.1, the fractural lateral displacement of a structural wall is taken as 2.0% of the drift ratio, and δ_u is accounted for 30% of the total displacement, given as equation (5).

$$\delta_u = h_w * 0.02 * 30\% \tag{5}$$

4. Fracture point (δ_a, V_a)

   According to TEASPA 3.1, the fractural lateral displacement of a structural wall is taken as 2.0% of the drift ratio. In this study, it is assumed that the sliding deformation account for 50% of the total displacement, given as equation (6).

$$\delta_a = h_w * 0.02 * 50\% \tag{6}$$

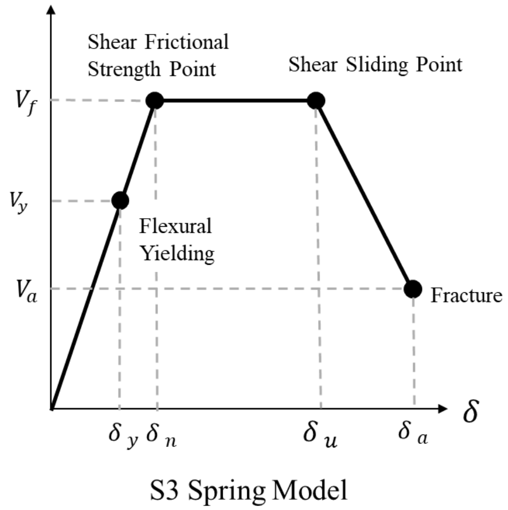

Fig. 4 Load-Deformation relationship of S3 sliding spring model

STRENGTH VALIDATION

ACI 318-14

According to ACI 318-14, Chapter 18.10, the nominal shear strength of a structural wall when under seismic loading should not exceed:

$$V_n = A_{cv}(\alpha_c \lambda \sqrt{f_c'} + \rho_t f_y) \tag{7}$$

Where A_{cv} is the gross area of concrete section bounded by web thickness and length of section in the direction of shear force, α_c is the coefficient of the relative contribution of concrete strength to nominal wall shear strength, and $\rho_t$is the reinforcing ratio of the transverse reinforcement.

Strut-and-Tie Model

According to Huang et al. (1999,2000), the softened strut-and-tie model has been developed to determine the shear strength of discontinuity regions of RC structures, particularly applied for predicting the strength of deep beams, corbels, squat walls, and beam-column joints, where failure modes were dominated by diagonal compression.

The force transfer mechanisms within the strut-and-tie model consist of three key components: the diagonal compressive strut between the compressed corner, the horizontal tie force, and the vertical tie force. The diagonal compressive strut can be estimated as:

$$C_{d,n} = K\zeta f_c' A_{str} \tag{8}$$

Where K denotes the strut-and-tie index; ζ represents the softening coefficient of cracked reinforced concrete and was calculated by equation (9); f_C' is the compressive strength of concrete, and the $A_{str}$is the effective area of the strut.

$$\zeta = \frac{3.35}{\sqrt{f_c'}} \leq 0.52\ (f_c'\ in\ MPa) \tag{9}$$

Considering the biaxial loading behavior of fiber reinforced concrete, the softening coefficient is suggested to be consider as equation (10)-(15).

$$\zeta = f(f_c')f(\overline{\varepsilon_1})f(\beta)W_p W f \leq 0.9 \tag{10}$$

Where

$$f(f_c') = \frac{5.8}{\sqrt{f_c'}} \leq 0.9\ (f_c'\ in\ MPa) \tag{11}$$

$$f(\overline{\varepsilon_1}) = \frac{1}{\sqrt{1+400\overline{\varepsilon_1}}} \tag{12}$$

$$f(\beta) = 1 - \frac{|\beta|}{24^{\circ}}, \beta = \frac{1}{2}\tan^{-1}\left[\frac{\gamma_{21}}{\varepsilon_2 - \varepsilon_1}\right] \tag{13}$$

$$W_p = 1.15 + \frac{|\beta|(0.09|\beta| - 1}{6} \tag{14}$$

$$Wf = 1 + 0.2FF, FF = (L_f ha/D_f)V_f \tag{15}$$

The FF in equation (15) denotes the aspect ratio of the fibers and the volume of fibers within the matrix.

Huang et al. (2017) proposed a geometric simplification of the strut-and-tie index K, which is determined by the strut's reinforcing ratio and the inclination angle θ. As the shear behavior in the D-region is highly sensitive to the inclination angle, the force transfer mechanism is categorized into two responses. For the specimen with $\theta \geq 45°$, the horizontal tie reinforcement dominates the mechanism, and the reinforcing ratio is taken as $\rho = \rho_h$. Conversely, when $\theta < 45°$ the vertical tie reinforcement dominates the mechanism, and the reinforcing ratio is taken as $\rho = \rho_v$. Hence, the strut-and-tie index K could be calculated by equations (16)-(17).

$$K = tan^A\,\theta + cot^A\,\theta - 1 + 0.14B \leq 1.64 \tag{106}$$

$$A = \frac{12\rho f_y}{f_c'} \leq 1\ ;\ B = \frac{30\rho f_y}{f_c'} \leq 1 \tag{117}$$

With the incorporation of ACI 318, Strut-and-Tie Model, and Modified Compression Field Theory, the shear strength was calculated and compared with the shear demand derived by cross-sectional analysis, as shown in Table 2. These predictions on the mechanical behavior of the squat shear wall were addressed and compared with the experimental and simulation outcomes.

Table 2. Shear strength of squat shear walls

	$V_{n,ACI}$	V_{SST}	V_{MCFT}	M_n/h_w
$\mathrm{HSC-HS}-0.83\sqrt{f_c'}$	1682 kN	1379 kN	1197 kN	2323 kN
$\mathrm{UHPC-HS}-0.7\sqrt{f_c'}$	1778 kN	1625 kN	1234 kN	2413 kN
$\mathrm{UHPC-SF-NS}-0.5\sqrt{f_c'}$	1201 kN	1358 kN	1726 kN	2283 kN
$\mathrm{UHPC-SF-HS}-0.7\sqrt{f_c'}$	1704 kN	1468 kN	1856 kN	2356 kN

SIMULATION RESULTS

This study conducted experiments and simulations on four squat shear walls with similar design configurations but incorporating different types of UHPC materials. As shown in Fig. 5, experimental results are represented by blue solid lines, while numerical simulations are denoted by red dashed lines.

Experimental results revealed that all four specimens failed in shear, and the steel fiber-reinforced shear walls exhibited higher toughness and achieved flexural strength.

$\mathrm{HSC-HS}-0.83\sqrt{\mathrm{f}_c'}$ and $\mathrm{UHPC-HS}-0.7\sqrt{\mathrm{f}_c'}$ were analyzed using the S1 and S2 sliding-shear spring models, with both models match well the experimental trends. In comparison, the addition of fibers significantly enhanced the shear strength and toughness of the specimen $\mathrm{UHPC-SF-NS}-0.5\sqrt{\mathrm{f}_c'}$ and $\mathrm{UHPC-SF-HS}-0.7\sqrt{\mathrm{f}_c'}$. Since the maximum strength is lower than shear frictional strength, shear sliding failure did not occur. As a result, the S3 sliding-shear failure lateral force-displacement curve proposed in this study underestimated lateral force and overestimated the sliding displacement. Nevertheless, the overall hysteresis loops of lateral force-displacement analyses reasonably aligned with the experimental trends.

Additionally, this study evaluated the predictive capabilities of existing design provisions, the strut-and-tie model, and the modified compression field theory (MCFT). The data showed that the calculated shear strength of three specimens, except for $\mathrm{UHPC-HS}-0.7\sqrt{\mathrm{f}_c'}$, was relatively conservative, with the strut-and-tie model consistently underestimating the strength by approximately 40%.

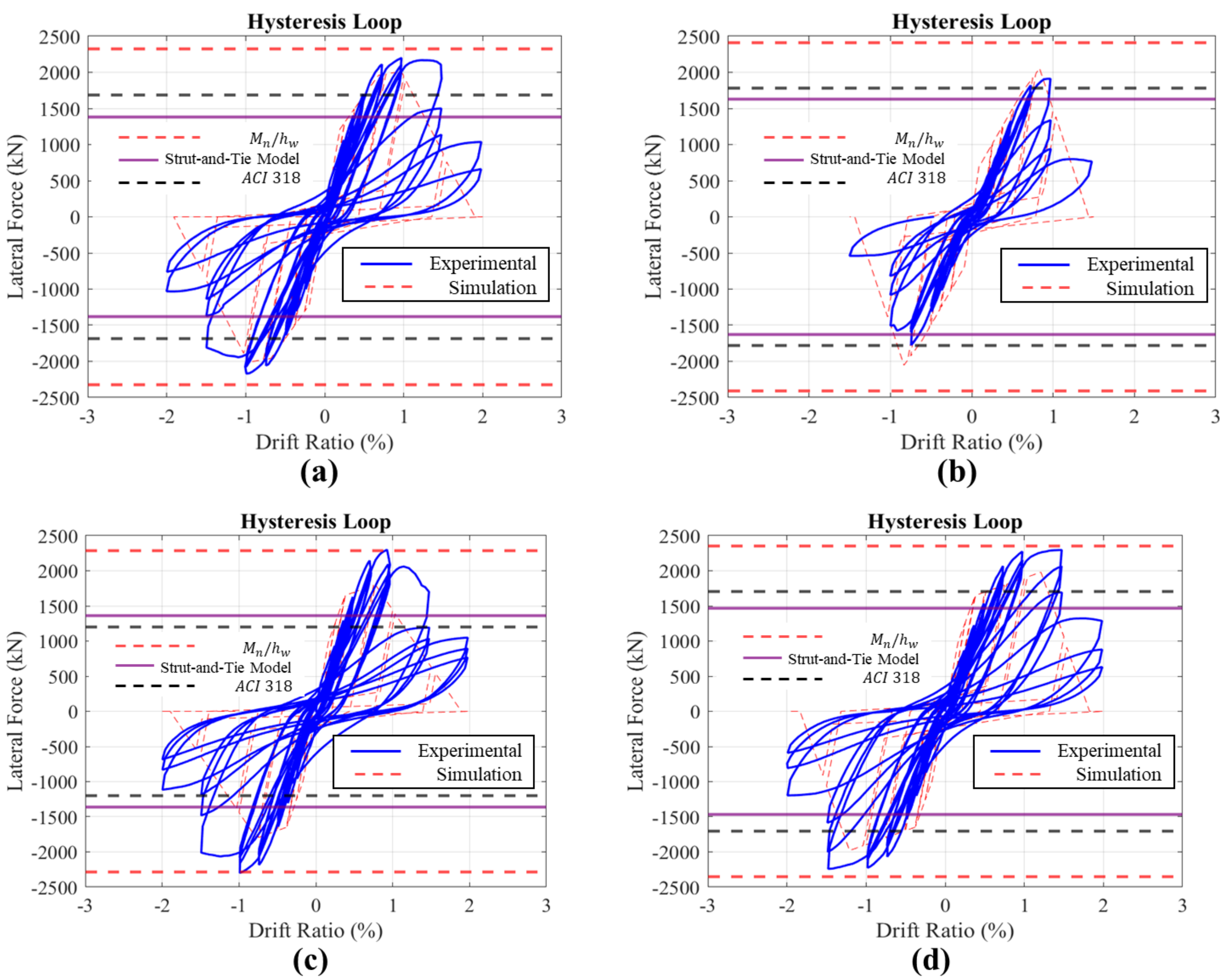

Fig. 5 Simulation and experimental results of (a) HSC-HS-0.83$\sqrt{f_c'}$ (b) UHPC-HS-0.7 $\sqrt{f_c'}$ (c) UHPC-SF-NS-0.5$\sqrt{f_c'}$ (d) UHPC-SF-HS-0.7$\sqrt{f_c'}$

CONCLUSION

In this study, the OpenSees model that incorporated a nonlinear beam element and zero-length element to reflect the flexural and shear response of squat shear walls was validated through experimental results. In the simulation model, cross sections of the squat shear walls were defined by fiber section, shear springs were derived from the modified compressive field theory, and the sliding shear behavior following TEASPA 3.1 and ACI 318 was considered. Findings demonstrated that the developed computational model reasonably captures the hysteretic behavior, including pinching effect, stiffness, strength, energy dissipation capacity, and shear sliding deformation of UHPC shear walls with different designing parameters. To conclude, the proposed model could efficiently capture the hysteretic behavior of the squat shear walls incorporated with high-strength materials, namely UHPC and high-strength reinforcement, and provide potential applications in designing and constructing shear walls.

REFERENCES

ACI Committee 318. (2015). Building Code Requirements for Structural Concrete (ACI 318-14): An ACI Standard: Commentary on Building Code Requirements for Structural Concrete (ACI 318R-14), an ACI Report. American Concrete Institute.

Bentz, E. C., Vecchio, F. J., and Collins, M. P. (2006). "Simplified Modified Compression Field Theory for Calculating Shear Strength of Reinforced Concrete Elements," ACI Structural Journal, 103(4).

Chiou, T.-C., Hsiao, F.-P., Chung, L.-L., Weng, J.-H., Li, C.-H., Liu, C.-C., Xue, Q., Ho, Y.-S., Chen, S.-J., Yang, C.-P., Weng, P.-W., Shen, W.-C., Tu, Y.-S., Yang, Y.-S., Li, Y.-A., Yeh, Y.-K., & Hwang, S.-J. (2018). "Taiwan Earthquake Assessment for Structures by Pushover Analysis (TEASPA V3.1)" (NCREE-18-015). National Center for Research on Earthquake Engineering (NCREE).

EN 1998-1 (2004), "Eurocode 8: Design of structures for earthquake resistance Part 1: General rules, seismic actions and rules for buildings, " CEN: European Committee for Standardization

Filippou, F.C., Popov, E.P., Bertero, V.V. (1983) "Effects of bond deterioration on hysteretic behavior of reinforced concrete joints," Report EERC 83-19, Earthquake Research Center, University of California, Berkeley.

Han T.S., Feenstra P.H., Billington S.L.(2003). "Simulation of Highly Ductile Fiber Reinforced Cement-ased Composite Components Under Cyclic Loading," ACI Structural Journal, 100(6), pp. 749-757.

Hung, C. C., & Hsieh, P. L. (2020). "Comparative study on shear failure behavior of squat high strength steel reinforced concrete shear walls with various high-strength concrete materials." In Structures, 23.

Hwang, S. J., and Lee, H. J. (1999), "Analytical model for predicting shear strengths of exterior reinforced concrete beam-column joints for seismic resistance," *ACI Structural Journal*, 96(5), 846–857

Hwang, S. J., and Lee, H. J. (2000), "Analytical model for predicting shear strengths of interior reinforced concrete beam-column joints for seismic resistance," *ACI Structural Journal*, 97(1), pp. 35–44

Hwang, S. J., Tsai, R.-J., Lam W.-K., Moehle, J. P. (2017), "Simplification of Softened Strut-and-Tie Model for Strength Prediction of Discontinuity Regions." *ACI Structural Journal*, 114(5).

Lehman, D. E. and Moehle, J. P. (2000), "Seismic Performance of Well-Confined Concrete Bridge Columns." Earthquake Engineering Research Center, Report 140 PEER1998/01, California, pp.295.

Paulay, T., Priestley, M. J. N., and Synge, A. J. (1982), " Ductility in earthquake resisting squat shear walls," *ACI Journal Proceedings*, 79(4).

S. Mazzoni, F. McKenna, M.H. Scott, G.L. Fenves, "OpenSees command language manual," Pacific Earthquake Engineering Research (PEER) Center, 2006.